

HD 285507b: AN ECCENTRIC HOT JUPITER IN THE HYADES OPEN CLUSTER

SAMUEL N. QUINN^{1,3}, RUSSEL J. WHITE¹, DAVID W. LATHAM², LARS A. BUCHHAVE², GUILLERMO TORRES², ROBERT P. STEFANIK², PERRY BERLIND², ALLYSON BIERYLA², MICHAEL C. CALKINS², GILBERT A. ESQUERDO², GABOR FÜRÉSZ², JOHN C. GEARY², ANDREW H. SZENTGYORGYI²

Submitted to ApJ October 25, 2013

ABSTRACT

We report the discovery of the first hot Jupiter in the Hyades open cluster. HD 285507b orbits a $V = 10.47$ K4.5V dwarf ($M_* = 0.734 M_\odot$; $R_* = 0.656 R_\odot$) in a slightly eccentric ($e = 0.086^{+0.018}_{-0.019}$) orbit with a period of $6.0881^{+0.0019}_{-0.0018}$ days. The induced stellar radial velocity corresponds to a minimum companion mass of $M_P \sin i = 0.917 \pm 0.033 M_{\text{Jup}}$. Line bisector spans and stellar activity measures show no correlation with orbital phase, and the radial velocity amplitude is independent of wavelength, supporting the conclusion that the variations are caused by a planetary companion. Follow-up photometry indicates with high confidence that the planet does not transit. HD 285507b joins a small but growing list of planets in open clusters, and its existence lends support to a planet formation scenario in which a high stellar space density does not inhibit giant planet formation and migration. We calculate the circularization timescale for HD 285507b to be larger than the age of the Hyades, which may indicate that this planet's non-zero eccentricity is the result of migration via planet-planet scattering. We also demonstrate a significant difference between the eccentricity distributions of hot Jupiters that have had time to tidally circularize and those that have not, which we interpret as evidence against Type II migration in the final stages of hot Jupiter formation. Finally, the dependence of the circularization timescale on the planetary tidal quality factor, Q_P , allows us to constrain the average value for hot Jupiters to be $7.8 \times 10^5 \lesssim Q_P \lesssim 3.5 \times 10^6$.

Subject headings: open clusters and associations: individual (Hyades, Melotte 25) — stars: individual (HD 285507) — planetary systems: formation

1. INTRODUCTION

The efforts of more than two decades of exoplanet searches have produced an incredible diversity of discoveries, many of which bear little similarity to planets in the Solar System. These discoveries provide valuable constraints for our theories of planet formation, which have evolved to explain the existence of the wide array of planetary systems observed. One such grouping of planets is the hot Jupiters, gas giant planets in short period orbits (defined herein as $M_P > 0.3 M_{\text{Jup}}$ and $P < 10$ days), which occur at rates of $\sim 1.2\%$ around Sun-like field stars (Wright et al. 2012). However, more than 60 years after their proposed existence (Struve 1952) and nearly 20 years after the first detection (Mayor & Queloz 1995), we still lack a complete description of the hot Jupiter formation process. It is believed that they form beyond the snow line (located at ~ 2.7 AU for the current-day Sun; e.g., Martin & Livio 2013) where there is a greater reservoir of solids with which to build a massive core (e.g., Kennedy & Kenyon 2008) before undergoing an inward migration process, but many questions remain to be answered.

While there are many mechanisms that could cause a gas giant planet to lose angular momentum and migrate inward (see a discussion in Ford & Rasio 2008), two leading ideas are via dynamical interactions with a circumstellar disk (“Type II” migration; Goldreich & Tremaine

1980; Lin & Papaloizou 1986) and gravitational scattering caused by other planets (“planet-planet scattering”; e.g., Rasio & Ford 1996; Juric & Tremaine 2008). Migration from disk interactions must occur while the gas disk is present (within ~ 10 Myr; Haisch et al. 2001) and is expected to preserve near-circular orbits, but if planet-planet scattering is the predominant migration mechanism, inward migration may take significantly longer and most hot Jupiters should initially possess non-zero eccentricity. Given the different timescales for the two migration mechanisms, one direct way to distinguish between them would be to search for hot Jupiters orbiting very young stars ($\lesssim 10$ Myr), but the enhanced activity associated with young stars presents significant challenges for such surveys (e.g., Bailey et al. 2012). Alternatively, the dynamical imprint of planet-planet scattering on the orbital eccentricity could provide a more accessible means to observationally constrain migration. Subsequent tidal circularization of the orbits erases this evidence of scattering over time, so identifying “dynamically young” systems, for which the system age (t_{age}) is less than the circularization timescale (τ_{cir}), is necessary for such an investigation. Longer period planets (large τ_{cir}) could satisfy this requirement, but hot Jupiters with periods of only a few days are both more common and easier to detect. Young planets (small t_{age}) offer another solution, but field stars tend to be old and their ages are difficult to estimate accurately (Mamajek & Hillenbrand 2008). The ages of open clusters, on the other hand, are typically precisely known and can be comparable to (or less than) the circularization timescales of many hot Jupiters, so planets in clusters could provide an avenue to

¹ Department of Physics & Astronomy, Georgia State University, 25 Park Place Suite 605, Atlanta, GA 30302

² Harvard-Smithsonian Center for Astrophysics, 60 Garden St, Cambridge, MA 02138

³ NSF Graduate Research Fellow

directly measure this observational signature of planet-planet scattering, allowing us to determine which process is most important for hot Jupiter migration. Throughout this paper, we explicitly discuss only Type II migration and planet-planet scattering, but we stress again that there are other multi-body dynamical processes, notably the Kozai effect (e.g., Fabrycky & Tremaine 2007), that may have the same qualitative effect on orbital eccentricity as planet-planet scattering. We revisit this briefly in the discussion.

With the recent discovery of two hot Jupiters (Quinn et al. 2012) in the Praesepe open cluster (~ 600 Myr), it is now clear that giant planets can form and migrate in a dense cluster environment. This had been an open question, as previous exoplanet surveys targeting open clusters – including high resolution spectroscopy of 94 dwarfs in the Hyades (Paulson et al. 2004) and 58 dwarfs in M67 (Pasquini et al. 2012), as well as transit photometry of several other clusters (e.g., Hartman et al. 2009; Pepper et al. 2008; Mochejska et al. 2006) – had not discovered any planets. However, while small planets do appear to be a common by-product of star formation, *giant* planets are comparatively rare (e.g., Fressin et al. 2013). Most cluster surveys have not been sensitive to the more common smaller planets, so it is likely that small sample sizes are to blame for the null results (see also van Saders & Gaudi 2011). Indeed, two mini-Neptunes recently discovered (Meibom et al. 2013) in NGC 6811 (~ 1 Gyr, Meibom et al. 2011) by the *Kepler* spacecraft would not have been detected by previous surveys, and the results suggest consistency between occurrence rates in open clusters and the field for planets of all sizes.

While open cluster planet surveys have recently enjoyed successes in measuring planet formation rates, they have not yet provided a convincing constraint for the hot Jupiter migration process, despite their potential to do so in the long term. Unfortunately, the hot Jupiters discovered in Praesepe are too old to address timescale differences between migration mechanisms, and they are not dynamically young, either. That is, they are close enough to their stars to have already undergone tidal circularization ($t_{\text{age}} > \tau_{\text{cir}}$). To see the dynamical imprint of migration it will thus be necessary to identify younger hot Jupiters or hot Jupiters on wider orbits that would still bear the signature of dynamical scattering in order to help distinguish between migration mechanisms. In hopes of accomplishing the latter, here we extend our radial velocity (RV) survey to include more stars with ages and properties comparable to those in Praesepe.

We describe our sample selection in § 2 and outline our spectroscopic and photometric observations and analysis in § 3 and § 4. We then present evidence for migration via scattering and a constraint on Q_P in § 5 through § 7, and in § 8 we discuss our results.

2. SAMPLE SELECTION

Hyades cluster members represent an ideal sample for extending our survey of Sun-like stars in Praesepe (Quinn et al. 2012). The two clusters are nearly the same age (625 Myr and 578 Myr, respectively; Perryman et al. 1998; Delorme et al. 2011), and both are metal-rich – $[\text{Fe}/\text{H}] = +0.13 \pm 0.01$ (Hyades, Paulson et al. 2003) and $+0.19 \pm 0.04$ (Praesepe, Quinn et al. 2012). While

Paulson et al. (2004) found no planets among 94 Hyades dwarfs, a primary motivation of their survey was to explore the relationship between planet occurrence and stellar mass, so a number of FGK stars were omitted in favor of including 20 M stars. As a result, some suitable stars have not yet been observed with precise radial velocities.

Our potential targets come from a list assembled by Robert Stefanik for the CfA Hyades binary survey (private communication). Since 1979, the CfA has been monitoring over 600 stars in the Hyades field, extending to a magnitude of $V = 15$. Originally the program consisted of stars drawn from the Hyades lists of van Bueren (1952), van Altena (1966), and Pels et al. (1975). Over the years additional stars were added to the observing program if there was some suggestion that the stars were possible members based on photometric, proper motion, or radial velocity investigations of the cluster. Also added to the CfA program were the companion stars of Hyades visual binaries. From this parent list, the sample surveyed here was determined after excluding close visual binaries revealed by high-resolution imaging (Patience et al. 1998), the 94 stars previously surveyed by Paulson et al. (2004), rapid rotators ($v \sin(i) > 30 \text{ km s}^{-1}$), faint targets ($V > 12$), and spectroscopic binaries from the literature and the CfA survey. The final target list contained 27 FGK Hyades members (see Table 1).

3. HIGH RESOLUTION SPECTROSCOPY

3.1. Spectroscopic Observations

The Tillinghast Reflector Echelle Spectrograph (TRES; Fűrész 2008) mounted on the 1.5-m Tillinghast Reflector at the Fred L. Whipple Observatory (FLWO) on Mt. Hopkins, AZ was used to obtain high resolution spectra of Hyades members between UT 2012 September 23 and 2013 April 08. TRES is a temperature-controlled, fiber-fed instrument with a resolving power of $R \sim 44,000$ and a wavelength coverage of $\sim 3850\text{-}9100 \text{ \AA}$, spanning 51 echelle orders.

In order to achieve a sensitivity to planets similar to that achieved for Praesepe stars, we strove to observe each star on two to three consecutive nights, followed by another two to three consecutive nights ~ 1 week later (see Quinn et al. 2012). This strategy, given the RV precision of TRES, is sensitive to planets with masses greater than about $0.5 M_{\text{Jup}}$ and periods up to 10 days. Though we were sometimes forced to deviate from the planned observing cadence because of weather and instrument availability, we were able to obtain at least 5 spectra of each of our 27 stars. Exposure times ranged from 1-25 minutes, yielding a typical SNR per resolution element of at least 40. We also obtained nightly observations of the nearby IAU RV standard stars HD 38230 (28° away) and HD 3765 (54°) to help track instrument stability and correct for any RV zero point drift. Precise wavelength calibration was established by obtaining ThAr emission-line spectra before and after each spectrum, through the same fiber as the science exposures.

3.2. Spectroscopic Reduction and Cross Correlation

Spectra were optimally extracted, rectified to intensity versus wavelength, and for each star the individual spectra were cross-correlated, order by order, using

TABLE 1
 TARGET LIST AND OBSERVATIONS SUMMARY

Star	Other Name	α (J2000)	δ (J2000)	V (mag)	N	σ_{obs} (m s ⁻¹)	$v \sin i$ (km s ⁻¹)
J202A	HIP 15300	03 : 17 : 22.6	+26 : 18 : 55	11.10	6	39.8	2.2
H24098C	HD 24098C	03 : 50 : 13.1	-01 : 31 : 08	11.20	9	40.3	0.9
L7	HD 283044	03 : 52 : 40.8	+25 : 48 : 16	11.10	5	12.9	2.0
G7-73C	...	04 : 01 : 12.8	+12 : 05 : 48	11.30	7	40.0	2.9
L15	HD 285507	04 : 07 : 01.0	+15 : 20 : 07	10.47	34	90.5	3.2
L18	HD 284155	04 : 08 : 36.0	+23 : 46 : 07	9.42	7	25.8	2.0
VB13	HD 26345	04 : 10 : 42.3	+18 : 25 : 24	6.59	5	78.8	28.7
VB14 ^a	HD 26462	04 : 11 : 20.2	+05 : 31 : 23	5.70	24	608.4	17.6
H111	HD 286589	04 : 14 : 51.7	+13 : 03 : 18	10.68	6	22.5	2.1
L26	HD 285630	04 : 17 : 25.0	+19 : 01 : 47	10.80	5	23.7	2.3
H210	HD 286693	04 : 19 : 36.9	+12 : 37 : 27	9.80	6	7.5	0.6
H246	HD 27561	04 : 21 : 34.7	+14 : 24 : 35	6.58	5	30.6	22.1
L38	...	04 : 24 : 07.2	+22 : 07 : 08	10.95	5	8.5	3.0
H342	HD 285742	04 : 25 : 00.1	+16 : 59 : 05	10.37	8	14.4	1.5
L58	HD 284455	04 : 26 : 47.3	+21 : 14 : 05	11.24	10	21.8	2.6
G7-227	HD 285765	04 : 27 : 56.7	+19 : 03 : 39	11.36	6	17.9	1.7
H422	HD 285804	04 : 28 : 10.6	+16 : 28 : 14	10.72	5	23.3	2.5
H469	HD 28406	04 : 29 : 30.0	+17 : 51 : 48	6.89	5	54.3	33.4
H472	HD 285805	04 : 29 : 30.9	+16 : 14 : 42	10.63	8	19.0	1.9
VB86	HD 28608	04 : 30 : 56.7	+10 : 45 : 07	7.03	5	55.1	30.0
G8-64	HD 284785	04 : 47 : 08.5	+20 : 52 : 58	9.77	6	28.8	4.3
AK2-1315	...	04 : 47 : 18.0	+06 : 27 : 12	11.35	7	7.0	2.0
VB116	HD 30505	04 : 49 : 03.0	+18 : 38 : 30	8.97	8	28.6	4.0
L96	HD 286085	04 : 50 : 00.4	+16 : 24 : 45	10.73	7	28.8	3.6
+23755	HD 284855	04 : 53 : 00.6	+23 : 29 : 18	10.61	7	15.2	1.7
L101	BD +13 741	04 : 57 : 00.4	+13 : 54 : 46	10.86	7	45.0	3.9
VB128	HD 31845	04 : 59 : 44.0	+15 : 55 : 03	6.75	5	47.9	34.9

^a VB14 has a blended composite spectrum with variation in at least one component, which induces an apparent RV variation of several km s⁻¹ on a timescale of weeks. It is likely a triple system consisting of a single-lined binary and a more distant, yet unresolved, companion.

the strongest exposure of that star as a template (for details, see Buchhave et al. 2010). We typically used ~ 25 orders, rejecting those plagued by telluric absorption, fringing far to the red, and low SNR far to the blue. For each epoch, the cross correlation functions (CCFs) from all orders were added and fit with a Gaussian to determine the relative RV for that epoch. Internal error estimates (which include, but may not be limited to, photon noise) for each observation were calculated as $\sigma_{\text{int}} = \text{RMS}(\vec{v})/\sqrt{N}$, where \vec{v} is the RV of each order, N is the number of orders, and RMS denotes the root-mean-squared velocity difference from the mean.

To evaluate the significance of any potential velocity variation, we compared the observed velocity dispersions (σ_{obs}) to the combined measurement uncertainties, which we assumed stem from three sources: (1) internal error, σ_{int} (described above), (2) night-to-night instrumental error, σ_{TRES} , and (3) RV jitter induced by stellar activity, σ_* .

Before assessing the instrumental error, we used observations of HD 38230 and HD 3765 to correct for any systematic velocity shifts between runs, calculated in the following way. First, the median RV of each of the two standard stars was calculated for each run, resulting in two sets of run-to-run offsets. We took the error-weighted mean of these offsets to be the final run-to-run offsets, which were then applied to our Hyades data. We note that the instrument has been remarkably stable during the span of our observations, with run-to-run offsets similar to their uncertainties, typically less than 3 m s⁻¹. After run-to-run corrections, the RMS of the standard star

RVs was 10.5 m s⁻¹ with internal errors of only 7.6 m s⁻¹. Since we expect negligible stellar jitter for the RV standards, the instrumental floor error should be given by $\sigma_{\text{TRES}} = \sqrt{\sigma_{\text{obs}}^2 - \sigma_{\text{int}}^2}$ m s⁻¹. Thus, we adopted a night-to-night instrumental error of $\sigma_{\text{TRES}} = 7.2$ m s⁻¹. In order to reduce identification of false signals caused by noisy stars, we set $\sigma_* = 16$ m s⁻¹ (the average value for the Hyades found by Paulson et al. 2004) in our initial analysis of the 27 Hyades stars.

Accounting for internal errors, instrumental jitter, and stellar noise, we constructed a χ^2 fit of each star's RVs assuming a constant velocity, and then calculated $P(\chi^2)$, the probability that the observed χ^2 value would arise from a star of constant RV. Given constraints imposed by telescope time, our threshold for further follow-up was $P(\chi^2) < 0.001$ (i.e., 99.9% confidence of variability). Two stars met this criterion. The first, HD 26462, initially showed variation suggestive of a planetary or brown dwarf companion (~ 1 km s⁻¹), but subsequent observations revealed a larger variation and a strong correlation between the line broadening and the radial velocities. We concluded that two sets of spectral lines were present and that the true variation is much larger than a few km s⁻¹, but diluted by the blended set of lines. HD 26462 is most likely a hierarchical triple system composed of a single-lined binary and a more distant stellar companion, and we will discuss it in more detail in a subsequent paper about the stellar populations of Praesepe and the Hyades. The second star to meet our variability threshold was HD 285507, which also stood out obviously by eye as having significant RV variations after just 3 ob-

TABLE 2
RELATIVE RADIAL VELOCITIES OF
HD 285507

BJD (-2456000)	RV (m s^{-1})	σ_{RV} (m s^{-1})
196.96928	42.3	10.0
207.93330	180.1	9.4
208.90481	61.6	10.7
209.86006	7.7	10.7
210.82123	92.9	9.3
211.89901	252.5	15.0
223.88429	198.3	7.0
224.83584	266.6	10.4
225.82361	228.3	8.0
226.83416	113.0	10.6
227.79041	16.9	7.6
228.80807	65.0	9.6
229.78857	179.7	9.3
234.94762	72.6	9.3
235.89156	167.1	8.0
236.82198	256.2	8.8
237.85251	226.8	9.2
238.92242	106.0	8.0
263.79884	85.0	8.6
264.81227	12.2	8.9
267.84157	257.2	8.5
268.94476	169.6	9.9
282.78804	1.3	8.5
283.74106	72.7	11.1
293.85762	100.8	7.2
325.71304	0.0	7.0
350.64048	96.2	10.0
351.70178	209.5	12.7
358.63303	249.5	8.8
362.68212	68.4	16.8
374.66505	7.5	9.5
390.62275	216.4	12.6

NOTE. — The errors listed here are internal error estimates, but in the orbital solution we include an instrumental floor error of 7.2 m s^{-1} , added in quadrature with the internal errors. No stellar jitter was required.

servations. We continued to monitor it over the rest of the season, obtaining 32 epochs spanning 194 days. The radial velocities are presented in Table 2, and we discuss the system in detail in the following sections.

3.3. Orbital Solution

We used a Markov Chain Monte Carlo (MCMC) analysis to fit Keplerian orbits to the radial velocity data of HD 285507, fitting for orbital period P , time of conjunction T_c , the radial velocity semi-amplitude K , the center-of-mass velocity γ_{rel} , and the orthogonal quantities $\sqrt{e} \cos \omega$ and $\sqrt{e} \sin \omega$, where e is eccentricity and ω is the argument of periastron. We adopted errors corresponding to the extent of the central 68.3% interval of the MCMC posterior distributions.

The RV errors did not require the addition of stellar jitter in order to obtain a good fit ($\chi_{\text{red}}^2 = 1$), so we set $\sigma_* = 0$ in the orbital solution. We report the best fit orbital parameters in Table 3 and plot the best fit orbit in Figure 1.

3.4. Tests for a False Positive

HD 285507 is slowly rotating ($P_{\text{rot}} = 11.98$ days; Delorme et al. 2011), no X-ray emission was detected by

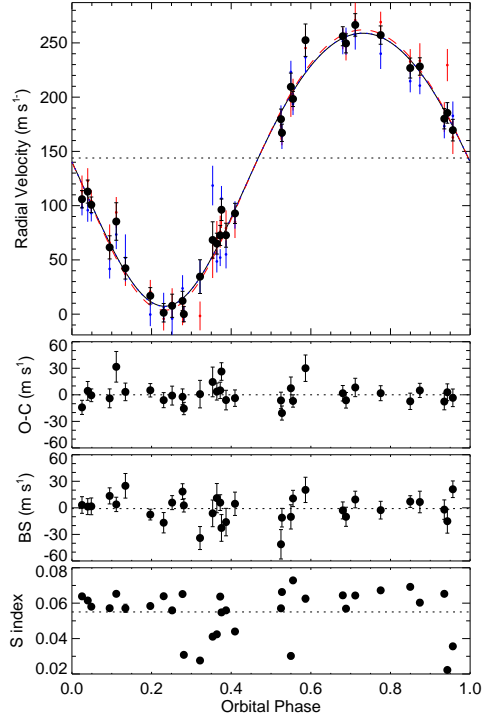


FIG. 1.— Orbital solution for HD 285507b. The panels, from top to bottom, show the relative RVs, best-fit residuals, bisector span variations, and relative S index values. In the top panel the large black points are the final RVs, but also plotted are the RVs derived from the blue and red orders of the spectrum, showing agreement at different wavelengths (see § 3.4). RV error bars represent the internal errors, and do not include astrophysical or instrumental jitter, although 7.2 m s^{-1} instrumental jitter was added to the orbital fit. The solid curve shows the best-fit orbital solution (and the blue and red dashed curves show the fits to the blue and red RVs). The orbital parameters are listed in Table 3.

ROSAT (Stern et al. 1995), and no stellar jitter term was required to obtain a good fit to the radial velocities, all of which are suggestive of a chromospherically inactive star. Nevertheless, to rule out false positive scenarios in which the observed RV variations are caused by stellar activity or stellar companions, we used our observations of HD 285507 to search for spectroscopic signatures that correlate with the orbital period.

If the RV variations were caused by a background blend (Mandushev et al. 2005) or star spots (Queloz et al. 2001), we would expect the shape of the star’s line bisector to vary in phase with the radial velocities. A standard prescription for characterizing the shape of a line bisector is to measure the relative velocity at its top and bottom; this difference is referred to as a line bisector span (see, e.g., Torres et al. 2005). To test against background blends or star spots, we computed the line bisector spans for all observations of HD 285507. As illustrated in Figure 1, the bisector span variations are small ($\sigma_{\text{BS}} = 15 \text{ m s}^{-1}$) and are not correlated with the observed RV variations.

For each spectrum we also computed the S index – an indicator of chromospheric activity in the Ca II H&K lines. We follow the procedure of Vaughan et al. (1978), but we note that our S indices are not calibrated to their scale; these are relative measurements. Correlation between S index and orbital phase might be expected if

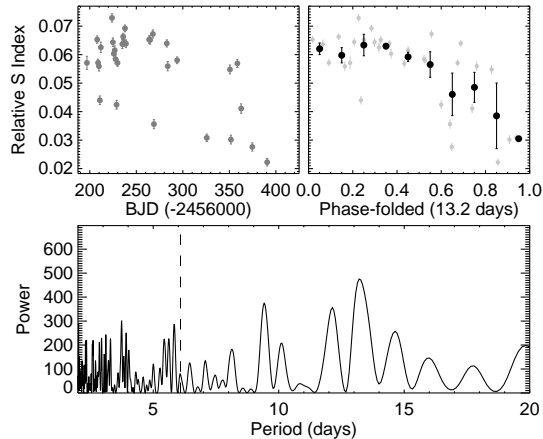


FIG. 2.— *Top left*: the stellar activity, as characterized by the relative S index measured from our spectra of HD 285507. *Bottom*: the Lomb-Scargle periodogram indicates that there may be significant periodicity on timescales similar to the stellar rotation period of 11.98 days (Delorme et al. 2011), but not at the RV period of 6.09 days (dashed line). *Top right*: the data have been folded onto the highest peak, 13.2 days, and binned for illustration.

the apparent RV variations were activity-induced, but as shown in Figure 1, there is no such correlation. Instead, there may be significant periodicity in the S indices at 12 or 13 days (Fig. 2), which is similar to the published rotation period of 11.98 days. Our data set is too sparse to claim a detection of the rotation period from the activity measurement, but we can see there is no power at the observed orbital period of 6.088 days.

Finally, if spots were the source of the variation, we would also expect the RV amplitude to be wavelength dependent because contrast between the spot and the stellar photosphere is wavelength dependent. We derived RVs for the blue and red orders separately (weighted mean wavelengths of $\lambda_{\text{blue}} = 4967 \text{ \AA}$ and $\lambda_{\text{red}} = 5845 \text{ \AA}$), and find the amplitudes to be consistent at the level of 0.5σ (3 ms^{-1} , Fig. 1). While the expected amplitude difference would be much greater, e.g., between the IR and the optical, the agreement between the red and blue amplitudes is encouraging.

We conclude from the evidence presented above that the observed RV variation is not caused by spots, but is the result of an orbiting planetary companion.

3.5. Stellar and Planetary Properties

We used the spectroscopic classification technique Stellar Parameter Classification (SPC; Buchhave et al. 2012) to determine the effective temperature T_{eff} , surface gravity $\log g$, projected rotational velocity $v \sin i$, and metallicity $[\text{m}/\text{H}]$ of HD 285507. In essence, SPC cross-correlates an observed spectrum against a grid of synthetic spectra, and uses the correlation peak heights to fit a 3-dimensional surface in order to find the best combination of atmospheric parameters ($v \sin i$ is fit iteratively since it is only weakly correlated to changes in the other parameters). We used the CfA library of synthetic spectra, which are based on Kurucz model atmospheres (Kurucz 1992) calculated by John Laird for a linelist compiled by Jon Morse. Like other spectroscopic classification techniques, SPC can be limited by degeneracy between parameters, notably T_{eff} , $\log g$, and $[\text{m}/\text{H}]$, but in this case we can enforce the known cluster metallic-

ity ($+0.13 \pm 0.01$, Paulson et al. 2003) to partially break that degeneracy.

To determine the physical stellar parameters, we utilized the Dartmouth (Dotter et al. 2008), Yonsei-Yale (Yi et al. 2001), and Padova (Girardi et al. 2000) stellar models. Applying an observational constraint on the size of the star – imposed indirectly by the spectroscopic T_{eff} , V magnitude ($V = 10.473 \pm 0.012$, Röser et al. 2011), and distance ($41.34 \pm 3.61 \text{ pc}$, van Leeuwen 2007) – and enforcing the age (625 Myr, Perryman et al. 1998) and metallicity of the Hyades, we determined the best fit mass and radius for each of the three isochrones. All three results agreed to within 3% in mass and 5% in radius, and although the resulting $\log g$ values indicated by the isochrones were consistent with the spectroscopically determined value, the temperatures were nominally discrepant at the 2σ level. It is possible that, for stars of this mass and age, the stellar models and/or SPC suffer from a systematic bias not reflected in the formal errors. Given that the exact stellar parameters have little bearing on the results presented in this paper, we choose to simply caution the reader and inflate the errors on stellar mass and radius by a factor of two. We adopted the mean mass and radius from the three isochrone fits ($M_* = 0.734 \pm 0.034 M_{\odot}$, $R_* = 0.656 \pm 0.054 R_{\odot}$), where the uncertainties listed here are the inflated statistical errors. Table 3 lists all of the stellar and planetary properties. We note that our adopted temperature (4503 K) is consistent with previous estimates of the spectral type (e.g., K5, Nesterov et al. 1995), and using the spectral type/temperature relations assembled in Kraus & Hillenbrand (2007), we estimate a more precise spectral type of HD 285507 to be K4.5.

4. STELLAR INCLINATION AND A SEARCH FOR TRANSITS

Since the rotation period of HD 285507 is 11.98 days and we have estimates for R_* and $v \sin i$, we can in principle calculate the inclination of the stellar spin axis. In practice, the fractional uncertainty on $v \sin i$ is large (not because the absolute uncertainty is large, but because the value is small), and the inclination can only be constrained to be $i > 72^\circ$. This does not exclude an edge-on stellar equator ($i = 90^\circ$), and because hot Jupiters orbiting cool stars ($\lesssim 6250 \text{ K}$) tend to be well-aligned with the stellar spin axis (see, e.g., Albrecht et al. 2012), an inclination of $\sim 90^\circ$ would make a transit more likely *a priori*. However, even an inclined stellar spin axis would not preclude transits of HD 285507, as there is evidence to suggest that young planets tend to be more misaligned than old planets (e.g., Triaud 2011). In addition to providing a radius measurement for HD 285507b, transits of this relatively young planet orbiting a cool star could be valuable to the interpretation of these intriguing correlations.

With this in mind, we conducted photometric monitoring of HD 285507 with KeplerCam on the FLWO 1.2-m telescope at the predicted time of conjunction on UT 07-Nov-2012. KeplerCam is a monolithic, $4\text{k} \times 4\text{k}$ Fairchild 486 chip with a $23' \times 23'$ FOV and a resolution of $0.''336 \text{ pixel}^{-1}$. We used a Sloan i filter with exposure times of 45 seconds and readout time of 12 seconds, obtaining a total of 334 images over 5.5 hours. We reduced the raw images using the IRAF package

TABLE 3
STELLAR AND PLANETARY PROPERTIES

Orbital Parameters	
P [days]	6.0881 ± 0.0018
T_c [BJD]	2456263.121 ± 0.029
K [m s^{-1}]	125.8 ± 2.3
e^a	0.086 ± 0.019
ω [deg] ^a	182 ± 11
γ_{rel} [m s^{-1}]	143.9 ± 1.6
γ_{abs} [km s^{-1}] ^b	38.149 ± 0.023
Physical Properties	
M_* [M_\odot] ^c	0.734 ± 0.034
R_* [R_\odot] ^c	0.656 ± 0.054
$T_{\text{eff},*}$ [K] ^c	4503^{+85}_{-61}
$\log g_*$ [dex] ^c	$4.670^{+0.051}_{-0.058}$
$v \sin i$ [km s^{-1}]	3.2 ± 0.5
$[Fe/H]$ [dex] ^c	$+0.13 \pm 0.01$
Age [Myr] ^c	625 ± 50
$M_P \sin i$ [M_{Jup}]	0.917 ± 0.033

^a The MCMC jump parameters included the orthogonal quantities $\sqrt{e} \cos \omega$ and $\sqrt{e} \sin \omega$, but we report the more familiar orbital elements e and ω .

^b The absolute center-of-mass velocity has been shifted to the RV scale of Nidever et al. (2002), on which the velocities of HD 3765 and HD 38230 are $-63.202 \text{ km s}^{-1}$ and $-29.177 \text{ km s}^{-1}$, respectively.

^c From the final isochrone fits (§ 3.5). $[Fe/H]$ and age were fixed to their known values (Paulson et al. 2003; Perryman et al. 1998).

`mscred`, and performed aperture photometry with `SEXtractor` (Bertin & Arnouts 1996).

The resulting light curve showed no sign of a transit, but to determine our detection sensitivity, we simulated transits – using the routines of Mandel & Agol (2002) and a quadratic limb darkening law from Claret et al. (2012) – and injected them into our observed data. For each injected transit, we compared the mean flux in transit (for all points between mid-ingress and mid-egress) to the mean flux out of transit. If the two differed by more than 1σ , we classified that transit as detected. From this, we can rule out a central transit of objects larger than $0.35 R_{\text{Jup}}$ (see Figure 3). If HD 285507b were to transit, then the derived minimum mass would be the true planetary mass. Under this assumption and using the mass-radius-flux relation from Weiss et al. (2013), we would then expect its radius to be $\sim 0.95 R_{\text{Jup}}$, much larger than our sensitivity limit. We can also rule out all transits of a $0.95 R_{\text{Jup}}$ planet with impact parameters $b < 1$ (i.e., all but the most extreme grazing transits). Using the final ephemeris, the transit center should have occurred 2.22 hours after our observations began ($T_c = 2456238.7686$ BJD), with an uncertainty of ~ 1 hour, so it is unlikely that a transit occurred outside our observing window.

5. EVIDENCE FOR DYNAMICAL SCATTERING OF HD 285507b

The discovery of a hot Jupiter in the Hyades open cluster brings the total number of short period giant planets in clusters to 3. Of these, however, HD 285507b is unique

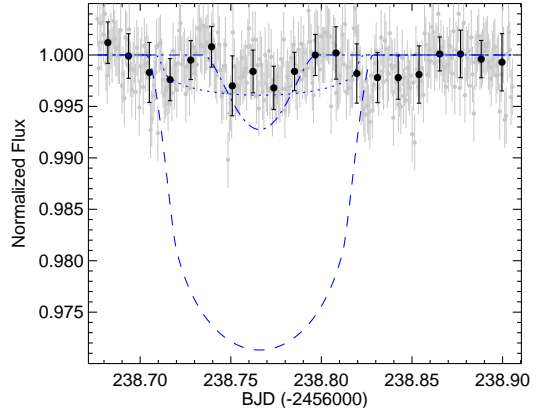


FIG. 3.— The light curve of HD 285507, showing the individual data (small grey circles), the binned data (large black circles), and three simulated transit models at the predicted time of transit (all of which are rejected as bad fits to the data): a central transit of a $0.95 R_{\text{Jup}}$ planet (dashed line), a central transit of a $0.35 R_{\text{Jup}}$ planet (dotted line), and a grazing transit ($b = 1$) of a $0.95 R_{\text{Jup}}$ planet (dash-dotted line). The latter two cases mark simulated detection limits for the observed data quality (see § 4).

in that it is the only one that is definitively eccentric; the 2 planets in Praesepe are consistent with having circular orbits. As described in the introduction, the non-zero eccentricity of HD 285507b could be a dynamical tracer of its migration history if the planet is dynamically young (i.e., $\tau_{\text{cir}} > t_{\text{age}} = 625$ Myr). If it is dynamically old, then the orbit should have already circularized, and establishing a credible link between the eccentricity and the migration process becomes more difficult – if the outer planet gets ejected during the planet-planet scattering event, as is expected, then one must invoke a separate mechanism to excite eccentricity again after circularization. To put it differently, if HD 285507b is dynamically young, then planet-planet scattering is sufficient (but not necessary) to explain the observations; if the planet is dynamically old, planet-planet scattering is neither sufficient nor necessary. To test these scenarios, we estimate τ_{cir} using the equation given by Adams & Laughlin (2006):

$$\tau_{\text{cir}} = 1.6 \text{ Gyr} \times \left(\frac{Q_P}{10^6} \right) \times \left(\frac{M_P}{M_{\text{Jup}}} \right) \times \left(\frac{M_*}{M_\odot} \right)^{-1.5} \times \left(\frac{R_P}{R_{\text{Jup}}} \right)^{-5} \times \left(\frac{a}{0.05 \text{ AU}} \right)^{6.5} \quad (1)$$

where Q_P is the planetary tidal quality factor (a measure of the efficiency of tidal dissipation within the planet). Note that τ_{cir} scales linearly with Q_P , which is unknown to within an order of magnitude. The Jupiter-Io interaction does provide the constraint $6 \times 10^4 < Q_{\text{Jup}} < 2 \times 10^6$ (Yoder & Peale 1981), but Q_P is likely dependent upon temperature, composition, rotation, and internal structure, all of which may be quite different for hot Jupiters. $Q_P \approx 10^6$, which we adopt herein, is a fiducial value often assumed for short period giant planets (for a more detailed discussion of tidal dissipation, see, e.g., Ogilvie & Lin 2004).

Since HD 285507b does not transit, we do not know R_P

and measure only a minimum mass, $M_P \sin i$. However, we can calculate the expectation value of $\sin i$ for randomly oriented orbits to determine the most likely mass, and then use the giant planet mass-radius-flux relation derived by Weiss et al. (2013) to estimate the planetary radius:

$$\frac{R_P}{R_\oplus} = 2.45 \left(\frac{M_P}{M_\oplus} \right)^{-0.039} \left(\frac{F}{\text{erg s}^{-1} \text{ cm}^{-2}} \right)^{0.094} \quad (2)$$

where F is the time-averaged incident flux on the planet. Since R_P depends only weakly on M_P , assuming an inclination is not likely to introduce a large radius error – there is only a 1% difference in derived radius between edge-on and average-inclination orientations.

Under these assumptions, we find $\tau_{\text{cir}} \approx 11.8$ Gyr – much larger than the age of the cluster. Note that this holds true even for the full range of Q_{Jup} (corresponding to $700 \text{ Myr} < \tau_{\text{cir}} < 22.6 \text{ Gyr}$). We conclude that HD 285507b is dynamically young. While it is tempting to thus proclaim that migration has occurred via planet-planet scattering, recall that this is not a necessary condition for a dynamically young planet with an eccentric orbit. For any individual planet, non-zero eccentricity could also be the result of continued interaction with an undetected planetary or stellar companion, a recent close stellar encounter, or even modest eccentricity excitation via Type II migration (e.g., D’Angelo et al. 2006). Only analysis of a population of planets can provide meaningful insight into the migration process in this manner. Therefore, we turn to the literature for ages and circularization timescales of the known sample of hot Jupiters.

6. EVIDENCE FOR DYNAMICAL SCATTERING AMONG KNOWN EXOPLANETS

To search for dynamical imprints of migration among known hot Jupiters ($M_P > 0.3 M_{\text{Jup}}$, $P < 10$ days), we follow the prescription described above to calculate τ_{cir} (and M_P and R_P for non-transiting planets). We adopt ages, eccentricities, planetary masses and radii, and stellar masses, radii, and temperatures from the literature.⁴ In Figure 4, we plot t_{age} versus τ_{cir} for this sample. While the figure is complicated by the uncertainties already discussed as well as poorly constrained ages and potential biases in measuring modest eccentricities (e.g., Pont et al. 2011; Zakamska et al. 2011), there is a hint that the points to the right of the circularization boundary are preferentially eccentric and the ones to the left are preferentially circular. If planet-planet scattering were the primary mechanism for the final stages of hot Jupiter migration, this would be expected; planets get scattered inward on highly eccentric orbits and circularize over time. If Type II migration were responsible, we should expect very little difference between the eccentricity distributions to the right and left of the boundary; ordered migration through a gas disk should largely preserve circular orbits, so subsequent tidal interactions would not change the population significantly. In Figure 5, we plot the eccentricity histograms and cumulative distributions for the two populations. To quantify the

⁴ All values were obtained from The Extrasolar Planets Encyclopaedia, www.exoplanet.eu. Only planets with ages listed on www.exoplanet.eu are included in this analysis.

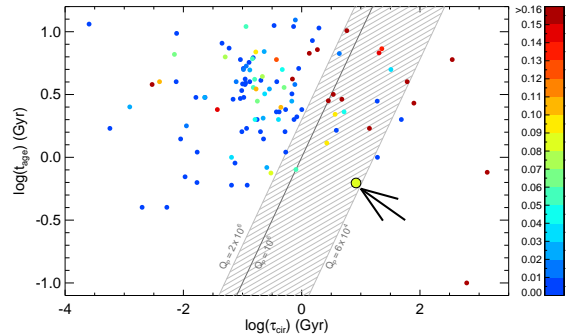


FIG. 4.— Age versus circularization timescale for short period ($P < 10$ days) massive ($M > 0.3 M_{\text{Jup}}$) planets, assuming a tidal quality factor $Q_P = 10^6$ for all planets. The solid dark line indicates where $t_{\text{age}} = \tau_{\text{cir}}$; planets to the left of the line are expected to have undergone tidal circularization. We also plot a shaded region to show the estimated uncertainty in this boundary given the range of Q_P values consistent with observations of the Jupiter-Io interaction (see Yoder & Peale 1981). The data points are colored according to their eccentricity, and HD 285507b is the large outlined circle indicated by the arrow. There is a hint that the right side is populated by preferentially eccentric (red) planets and the left side by preferentially circular (blue) planets. This is explored further in Figure 5.

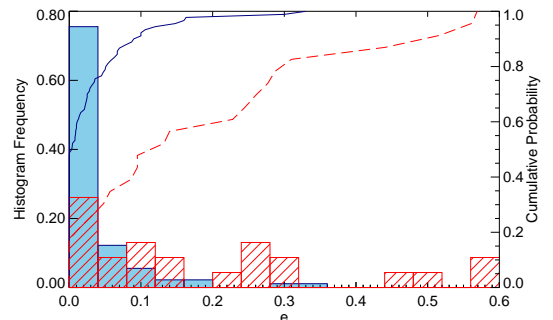


FIG. 5.— Eccentricity histograms and cumulative distributions of hot Jupiters that have (filled blue; left of the thick solid line in Fig. 4) and have not (striped red; right of the line) been tidally circularized. As in Figure 4, we have assumed $Q_P = 10^6$ for all planets. A KS test rejects the hypothesis that the two subsamples are drawn from the same distribution with 99.997% confidence. We interpret this to mean that the final stages of hot Jupiter migration tend to excite eccentricity, pointing toward planet-planet scattering as a likely cause.

difference between them, we ran a Kolmogorov-Smirnov (KS) test. The KS p-value is the likelihood that the two subsamples came from the same parent distribution, and in this case, $p = 3.3 \times 10^{-5}$. We conclude that the two distributions do not come from the same parent distribution, with $\sim 99.997\%$ confidence, and infer that planet-planet scattering plays a significant role in hot Jupiter migration.

7. A CONSTRAINT ON THE TIDAL QUALITY FACTOR Q FOR HOT JUPITERS

Note that until now we have been assuming $Q_P = 10^6$ to determine which planets are dynamically young (right side of the circularization boundary in Fig. 4) and which are dynamically old (left side), allowing us to draw conclusions about the migration process. If we instead *start* with the assumption that planets are scattered inward onto initially eccentric orbits (rather than gently shep-

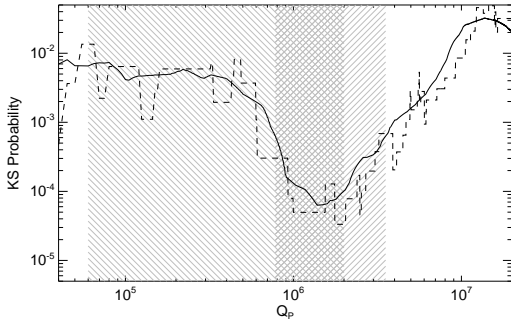


FIG. 6.— KS p-values for various assumed Q_P values (dashed line) and the smoothed distribution (solid line). Changing Q_P will shift the points left and right in Fig. 4, and thus change the distributions in Fig. 5. If we assume that the minimum p-value should occur for the most realistic Q_P (see § 7), then we can constrain the typical hot Jupiter Q_P value to be between about 7.8×10^5 and 3.5×10^6 (right shaded region encompassing the broad minimum). The Jupiter-Io constraint (left shaded region) only overlaps partially with the position of the minimum at $Q_P = 1.39 \times 10^6$, and given the expectation that Q will be larger for hot Jupiters, we do not apply this constraint to our adopted range for Q_P . Note also that the vertical axis is *not* a probability associated directly with Q_P , and should not be used as a quantitative measure.

herded on circular orbits through the gas disk), we can invert the problem to place a constraint on the tidal quality factor Q_P . As we vary Q_P , the circularization boundary changes location, and the difference between the two populations should be maximized (and the KS p-value minimized) for the correct (average) hot Jupiter Q_P . Note that it does not matter what fraction of hot Jupiters has undergone planet-planet scattering – if any fraction has, then the minimum p-value should occur when the circularization boundary is in the correct place. Figure 6 shows the results of this experiment. A value on the order of 10^6 is preferred, which seems to rule out much of the parameter space consistent with Jupiter’s tidal quality factor (and validates our assumption of $Q_P = 10^6$). The discrete data points do not produce a smooth distribution, so finding the minimum is not straightforward. As such, we smooth it using a moving average with a boxcar filter of size $[\frac{2}{3}Q_P, \frac{3}{2}Q_P]$. Quantitative confidence limits on the minimum are difficult to assess, but we take approximate upper and lower limits on Q_P to be those for which the smoothed p-value is 10 times its smoothed minimum value, which occurs for $Q_P = 1.39 \times 10^6$. While we caution that significant uncertainties remain that are not captured by these informal errors (especially potential biases in the published ages and eccentricities of known planets), we conclude that an appropriate tidal quality factor for a typical hot Jupiter is $\log Q_P = 6.14^{+0.41}_{-0.25}$ (see Fig. 6 for a visual representation).

8. SUMMARY AND CONCLUSIONS

Our discovery of a hot Jupiter in the Hyades bolsters the statistics of short period giant planets in open clusters (of which three are now known). Including the Paulson et al. (2004) null result in the Hyades (0 planets among 74 FGK stars), our Hyades sample (1 in 26), and an updated census of Praesepe including unpublished data from our second year of observations (2 in 60), a total of 3 out of 160 stars host a hot Jupiter. Af-

ter correcting for completeness and calculating Poisson errors following the prescription in Gehrels (1986), we find a hot Jupiter frequency of $1.97^{+1.92}_{-1.07}\%$ in the metal-rich Praesepe and Hyades open clusters. However, there is a well-known relationship between planet occurrence and metallicity (scaling approximately as $10^{1.2[\text{Fe}/\text{H}]}$; Johnson et al. 2010). If we take $[\text{Fe}/\text{H}] \approx +0.15$ as representative of the combined Praesepe and Hyades sample, the solar-metallicity-adjusted hot Jupiter frequency in clusters is $1.30^{+1.27}_{-0.71}\%$. Although more discoveries are needed to reduce the uncertainty, this is in good agreement with the frequency for field stars ($1.20 \pm 0.38\%$; Wright et al. 2012), and improves the evidence that planet frequency is the same in clusters and the field.

A primary motivation for the search for young planets is that their ages are comparable to the timescale of migration. Thus, the orbital properties of such planets may still bear the dynamical signature of this process. Since different migration mechanisms are predicted to produce hot Jupiters on different timescales and with different orbital eccentricities, we can use the properties of young hot Jupiters (and their existence at various ages) to determine the process by which they migrate. The ages of the cluster planets discovered thus far do not place a strong direct constraint on the *timescale* of migration (we know only that the process took less than 600 Myr), but the newly discovered planet in the Hyades holds a clue its dynamical history. HD 285507b has a long circularization timescale, so its non-zero eccentricity may be a remnant of the migration process, which would suggest that planet-planet scattering has played a role in its orbital evolution.

Applying this idea more broadly, we have compared ages and circularization timescales for all known hot Jupiters and find evidence for two families of planets, distinguished by their orbital properties: (1) mostly circular orbits for the “dynamically old” planets, those with $\tau_{\text{cir}} < t_{\text{age}}$, and (2) a range of eccentricities for “dynamically young” planets, those with $\tau_{\text{cir}} > t_{\text{age}}$. If Type II migration were the leading driver of hot Jupiter migration, both dynamically young and old planets should have circular orbits. We thus conclude that planet-planet scattering is important for giant planet migration. However, we can only say that these planets have experienced dynamical stirring *at some point*, and do not suggest that this evidence shows Type II migration to be unimportant. On the contrary, as shown by simulations time and again, Type II migration is almost certainly important to orbital evolution before the gas disk dissipates, but we suggest that for a large fraction of hot Jupiter systems, planet-planet scattering is responsible for the final stages of inward migration. A larger sample of dynamically young (non-circularized) planets may allow us to determine what that fraction is. Since few hot Jupiters have circularization timescales greater than 1 Gyr, a good way to enhance this sample is to continue finding young planets.

That dynamical scattering plays an important role in hot Jupiter migration has already been suggested, and is supported by a rich data set of stellar obliquity measurements in hot Jupiter systems (see Albrecht et al. 2012, for a recent discussion). In addition to the excitation of

orbital eccentricity, dynamical encounters with a third body are expected to produce a range of orbital inclinations, although tidal interactions with the host star may realign the systems over time. These inclinations can be measured precisely, most notably via the Rossiter-McLaughlin effect (Rossiter 1924; McLaughlin 1924), and the results of such studies parallel those presented in this paper: systems for which the tidal timescale is short tend to be well-aligned, and those for which the timescale is long display high obliquities. Albrecht et al. (2012) do caution that stars and their disks may be primordially misaligned for reasons unrelated to hot Jupiters, but we see no obvious reason for this to influence the eccentricities. Migration through multi-body dynamical interactions, on the other hand, could explain both the inclined orbits and high eccentricities observed in systems that have not yet experienced significant tidal interactions. Whether that process is primarily planet-planet scattering or the Kozai effect remains to be determined, and it is likely that more data will be needed to properly answer this question.

Finally, the tidal circularization boundary that separates the dynamically young and old populations of hot Jupiters is sensitive to the choice of the planetary tidal quality factor, Q_P , so we have leveraged this dependence to constrain the typical value for hot Jupiters to be $\log Q_P = 6.14_{-0.25}^{+0.41}$. Q_P has wide-ranging implications, e.g., for simulating orbital evo-

lution (Beaugé & Nesvorný 2012) or modeling the inflated radii of hot Jupiters (Bodenheimer et al. 2003), but has thus far proven difficult to constrain observationally. While our result still includes substantial uncertainty and will not be applicable to any one planet, it can be applied to these problems in a statistical sense. Moreover, it offers a path forward: as our sample of longer period and young hot Jupiters grows, the determination of Q_P using this method should improve.

We thank Tsevi Mazeh for insightful discussion, and Greg Feiden for producing a Dartmouth isochrone appropriate for our analysis. This research has made use of The Extrasolar Planets Encyclopaedia. The material herein is based upon work supported by the National Aeronautics and Space Administration (NASA) under Grant No. NNX11AC32G issued through the Origins of Solar Systems program. S. N. Q. is supported by an NSF Graduate Research Fellowship, Grant DGE-1051030. D. W. L. acknowledges partial support from NASA's Kepler mission under Cooperative Agreement NNX11AB99A with the Smithsonian Astrophysical Observatory. G. T. acknowledges partial support from NSF grant AST-1007992.

Facilities: FLWO:1.5m (TRES), FLWO:1.2m (Kepler-Cam)

REFERENCES

- Adams, F. C., & Laughlin, G. 2006, *ApJ*, 649, 1004
 Albrecht, S., Winn, J. N., Johnson, J. A., et al. 2012, *ApJ*, 757, 18
 Bailey, J. I., III, White, R. J., Blake, C. H., et al. 2012, *ApJ*, 749, 16
 Beaugé, C., & Nesvorný, D. 2012, *ApJ*, 751, 119
 Bertin, E., & Arnouts, S. 1996, *A&AS*, 117, 393
 Bodenheimer, P., Laughlin, G., & Lin, D. N. C. 2003, *ApJ*, 592, 555
 Buchhave, L. A., Bakos, G. Á., Hartman, J. D., et al. 2010, *ApJ*, 720, 1118
 Buchhave, L. A., Latham, D. W., Johansen, A., et al. 2012, *Nature*, 486, 375
 Claret, A., Hauschildt, P. H., & Witte, S. 2012, *A&A*, 546, 14
 D'Angelo, G., Lubow, S. H., & Bate, M. R. 2006, *ApJ*, 652, 1698
 Delorme, P., Collier Cameron, A., Hebb, L., et al. 2011, *MNRAS*, 413, 2218
 Dotter, A., Chaboyer, B., Jevremović, D., et al. 2008, *ApJS*, 178, 89
 Fabrycky, D., & Tremaine, S. 2007, *ApJ*, 669, 1298
 Ford, E. B., & Rasio, F. A. 2008, *ApJ*, 686, 621
 Fűrész, G. 2008, Ph.D. thesis, University of Szeged, Hungary
 Fressin, F., Torres, G., Charbonneau, D., et al. 2013, *ApJ*, 766, 81
 Gehrels, N. 1986, *ApJ*, 303, 336
 Girardi, L., Bressan, A., Bertelli, G., & Chiosi, C. 2000, *A&AS*, 141, 371
 Goldreich, P., & Tremaine, S. 1980, *ApJ*, 241, 425
 Haisch, K. E., Jr., Lada, E. A., & Lada, C. J. 2001, *ApJL*, 553, 153
 Hartman, J. D., Gaudi, B. S., Holman, M. J., et al. 2009, *ApJ*, 695, 336
 Johnson, J. A., Aller, K. M., Howard, A. W., & Crepp, J. R. 2010, *PASP*, 122, 905
 Juric, M., & Tremaine, S. 2008, *ApJ*, 686, 603
 Kennedy, G. M., & Kenyon, S. J. 2008, *ApJ*, 673, 502
 Kraus, A. L., & Hillenbrand, L. A. 2007, *AJ*, 134, 2340
 Kurucz, R. L. 1992, *IAUS*, 149, 225
 Lin, D. N. C., & Papaloizou, J. 1986, *ApJ*, 309, 846
 Mamajek, E. E., & Hillenbrand, L. A. 2008, *ApJ*, 687, 1264
 Mandel, K., & Agol, E. 2002, *ApJL*, 580, 171
 Mandushev, G., Torres, G., Latham, D. W., et al. 2005, *ApJ*, 621, 1061
 Martin, R. G., & Livio, M. 2013, *MNRAS*, 434, 633
 Mayor, M., & Queloz, D. 1995, *Nature*, 378, 355
 McLaughlin, D. B. 1924, *ApJ*, 60, 22
 Meibom, S., Barnes, S. A., Latham, D. W., et al. 2011, *ApJL*, 733, 9
 Meibom, S., Torres, G., Fressin, F., et al. 2013, *Nature*, 499, 7456
 Mochejska, B. J., Stanek, K. Z., Sasselov, D. D., et al. 2006, *AJ*, 131, 1090
 Nesterov, V. V., Kuzmin, A. V., Ashimbaeva, N. T., et al. 1995, *A&AS*, 110, 367
 Nidever, D. L., Marcy, G. W., Butler, R. P., et al. 2002, *ApJS*, 141, 503
 Ogilvie, G. I., & Lin, D. N. C. 2003, *ApJ*, 610, 477
 Pasquini, L., Brucalassi, A., Ruiz, M. T., et al. 2012, *A&A*, 545, 139
 Patience, J., Ghez, A. M., Reid, I. N., et al. 1998, *AJ*, 115, 1972
 Paulson, D. B., Sneden, C., & Cochran, W. D. 2003, *AJ*, 125, 3185
 Paulson, D. B., Cochran, W. D., & Hatzes, A. P. 2004, *AJ*, 127, 3579
 Pels, G., Oort, J. H., & Pels-Kluyver, H. A. 1975, *A&A*, 43, 423
 Pepper, J., Stanek, K. Z., Pogge, R. W., et al. 2008, *AJ*, 135, 907
 Perryman, M. A. C., Brown, A. G. A., Lebreton, Y., et al. 1998, *ã*, 331, 81
 Pont, F., Husnoo, N., Mazeh, T., & Fabrycky, D. 2011, *MNRAS*, 414, 1278
 Queloz, D., Henry, G. W., Sivan, J. P., et al. 2001, *A&A*, 379, 279
 Quinn, S. N., White, R. J., Latham, D. W., et al. 2012, *ApJL*, 756, 33
 Rasio, F. A., & Ford, E. B. 1996, *Science*, 274, 954
 Röser, S., Schilbach, E., Piskunov, A. E., et al. 2011, *A&A*, 531, 92
 Rossiter, R. A. 1924, *ApJ*, 60, 15
 Stern, R. A., Schmitt, J. H. M. M., & Kahabka, P. T. 1995, *ApJ*, 448, 683
 Struve, O. 1952, *Obs*, 72, 199
 Torres, G., Konacki, M., Sasselov, D. D., & Jha, S. 2005, *ApJ*, 619, 558
 Triand, A. H. M. J. 2011, *A&A*, 534, 6
 van Altena, W. F. 1966, *AJ*, 71, 482
 van Bueren, H. G. 1952, *Bull. Astron. Inst. Netherlands*, 11, 385
 van Leeuwen, F. 2007, *A&A*, 474, 653
 van Saders, J. L., & Gaudi, B. S. 2011, *ApJ*, 729, 63
 Vaughan, A. H., Preston, G. W., & Wilson, O. C. 1978, *PASP*, 90, 267
 Weiss, L. M., Marcy, G. W., Rowe, J. F., et al. 2013, *ApJ*, 768, 14
 Wright, J. T., Marcy, G. W., Howard, A. W., et al. 2012, *ApJ*, 753, 160
 Yi, S., Demarque, P., Kim, Y.-C., et al. 2001, *ApJS*, 136, 417
 Yoder, C. F., & Peale, S. J. 1981, *Icarus*, 47, 1
 Zakamska, N. L., Pan, M., & Ford, E. B. 2011, *MNRAS*, 410, 1895